

TITLE THE VERTEX DETECTOR FOR THE LEPTON/PHOTON COLLABORATION

AUTHOR(S) John P. Sullivan, Jan G. Boissevain, Dan Fox,
Barbara V. Jacak, Jon S. Kapustinsky, Michael J. Leitch,
Patrick L. McGaughey, Joel Moss, Walter E. Sondheim,
Hubert van Hecke


SUBMITTED TO Symposium on RHIC Detector R&D, Brookhaven National
Laboratory, Upton, NY, October 10-11, 1991

DISCLAIMER

This report was prepared as an account of work sponsored by an agency of the United States Government. Neither the United States Government nor any agency thereof, nor any of their employees, makes any warranty, express or implied, or assumes any legal liability or responsibility for the accuracy, completeness, or usefulness of any information, apparatus, product, or process disclosed, or represents that its use would not infringe privately owned rights. Reference herein to any specific commercial product, process, or service by trade name, trademark, manufacturer, or otherwise does not necessarily constitute or imply its endorsement, recommendation, or favoring by the United States Government or any agency thereof. The views and opinions of authors expressed herein do not necessarily state or reflect those of the United States Government or any agency thereof.

By acceptance of this article the publisher recognizes that the U.S. Government retains a nonexclusive, royalty-free license to publish or reproduce the published form of this contribution or to allow others to do so for U.S. Government purposes.

Los Alamos National Laboratory requests that the publisher identify this article as work performed under the auspices of the U.S. Department of Energy.

 Los Alamos National Laboratory
Los Alamos, New Mexico 87545

THE VERTEX DETECTOR FOR THE LEPTON/PHOTON COLLABORATION

J. P. Sullivan, J. G. Boissevain, D. Fox, H. van Hecke
B. V. Jacak, J. S. Kapustinsky, M. J. Leitch,
P. L. McGaughey, J. M. Moss, W. E. Sondheim
Physics Division, MS D456
Los Alamos National Lab
Los Alamos, NM 87545

Abstract

The conceptual design of the vertex detector for the Lepton/Photon Collaboration at RHIC is described, including simulations of its expected performance. The design consists of two concentric layers of single-sided Si strips. The expected performance as a multiplicity detector and in measuring the pseudo-rapidity (η) distribution is discussed as well as the expected vertex finding efficiency and accuracy. Various options which could be used to reduce the cost of the detector are also discussed.

1 Introduction and Design Assumptions

A vertex detector, based on silicon strips¹, was designed for the lepton/photon spectrometer collaboration². The purposes of the vertex detector were to measure the number of charged particles per unit pseudo-rapidity ($dN/d\eta$) and their multiplicity in addition to finding the vertex. A large part of the R&D that went into this design should be useful for any RHIC experiment.

In order to cover the central rapidity ($\approx \eta$) region, the $dN/d\eta$ measurement should cover η from ≈ -3 to $+3$. The total charged particle multiplicity must be available for the first level trigger. When the multiplicity is low, an accurate measurement requires a detector which covers a large fraction of the total solid angle. For central Au+Au collisions at RHIC the expected³ number of charged particles in the range $-3 < \eta < 3$ is around 5000. If the occupancy is to be kept

to 10% or less, this implies that the detector will need at least 50K channels in each layer.

Finally, the vertex detector must find the vertex. This should be done approximately (to within $\approx 1\text{cm}$) at the trigger level, with a more accurate determination ($\approx 1\text{mm}$) offline. Any vertex finding algorithm requires several charged particles in the detector, which is not a serious constraint for Au+Au collisions. However, in order to consistently find the vertex position for p+Au and p+p collisions, where the charged particle multiplicities can be much lower, a large fraction of the total solid angle must be covered.

2 Vertex Detector Conceptual Design

The conceptual design of the vertex detector was based on two concentric, approximately cylindrical, barrels of single-sided $300\mu\text{m}$ thick silicon strips with $100\mu\text{m}$ pitch². Fig. 1 shows schematic views. Half of the strips in each barrel are oriented parallel to z (the beam direction) and half orthogonal to z . The parallel and perpendicular strips are sometimes called “ r - ϕ ” and “ z ” strips, respectively.

The inner and outer detectors should not move relative to one another; details of these constraints are discussed in a later section. The detector should be constructed from “ladders” which maintain accurate relative positioning of the inner and outer detector wafers in each azimuthal segment. Each ladder will be constructed from Rohacell[®] foam⁴, which is a very light (reduces multiple scattering) but rigid foam whose coefficient of thermal expansion is close to that of Si. Using a ladder-like structure, rather than a solid piece of foam, further reduces the mass of the support structure and permits better airflow for cooling. Based on the expected power dissipation of the chips, preamps, and transmitters, the assembly will be air-cooled.

The ladders fit into a graphite/epoxy mechanical structure with a small coefficient of thermal expansion. The thermal expansion of the different pieces of the detector must be considered to maintain position accuracy. A large mismatch in the coefficients of thermal expansion of the detector wafers and the support structure could also result in severe damage to the detector. The modular construction of the detector allows some azimuthal segments to be removed if necessary.

A series of simulations of the detector were performed, using a nearly realistic model. The model was a pair of cylinders, whereas the “real” detectors² have a hexagonal cross-section. The “real” detector has dead areas around the edges of the chips, but in the simulations, the chips are assumed to be active even at their edges. Table 1 summarizes the number of channels assumed in the simulations of the vertex detector. For the chips containing strips parallel

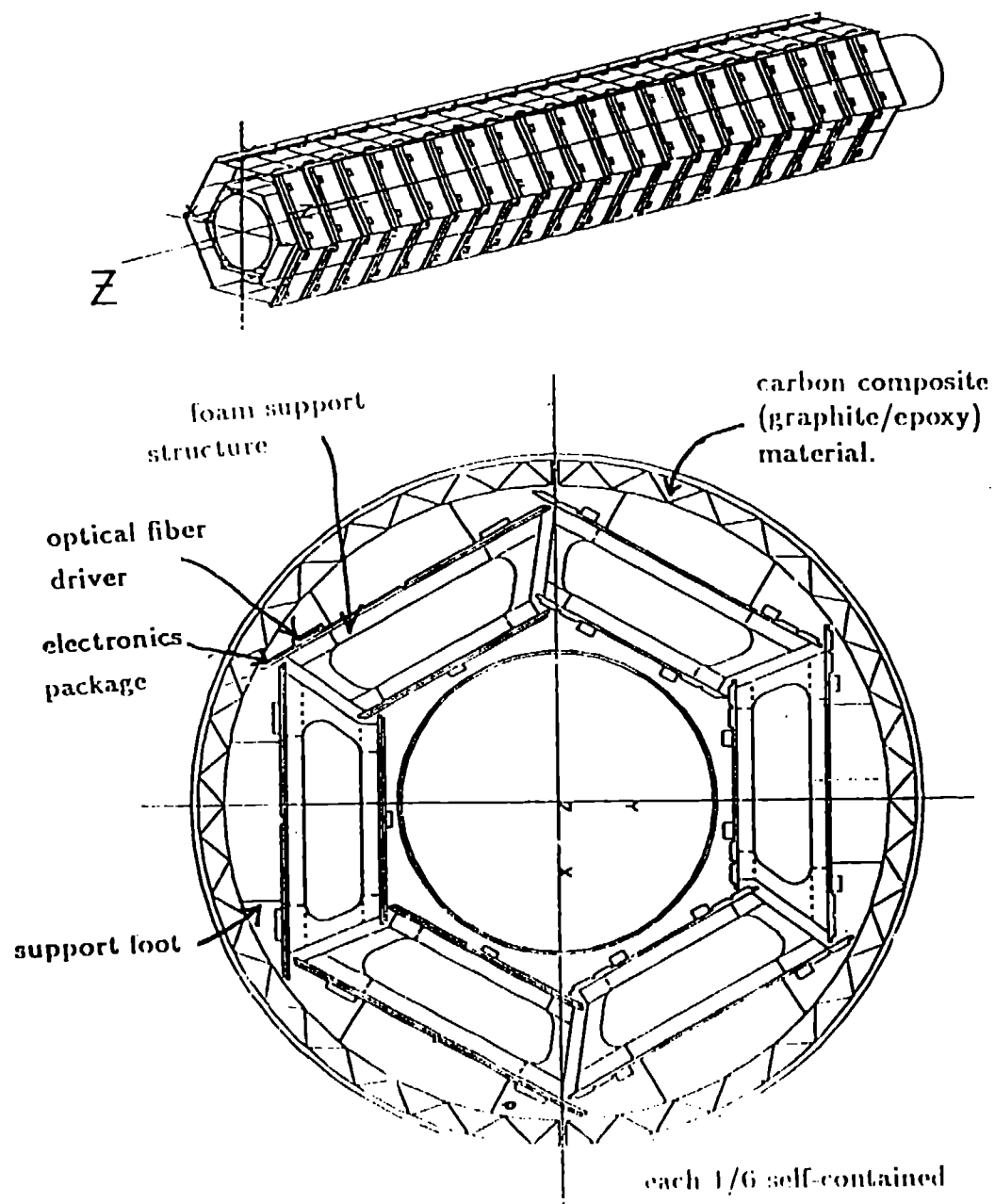


Figure 1: The conceptual design of the vertex detector. The bottom part shows the view along the beam line. The top part shows a 3D perspective view.

barrel	strip type	R (mm)	wafer size (mm x mm)	ϕ segments	# of wafers	strips/wafer	total strips
inner		61.1	64 x 50	3	20	640	38400
inner	\perp	61.1	32 x 50	3	40	480	57600
outer		91.7	96 x 50	3	40	320	38400
outer	\perp	91.7	48 x 50	3	40	480	57600
Totals					140		192000

Table 1: Summary of the number of channels in the simulation of the vertex detector. The shape is approximated by a cylinder, whose radius is given. Pitch= $100\mu m$ except parallel strips in the outer barrel, where $150\mu m$ is assumed

to the beam, there are some further differences between the simulations and a realistic design. The simulations assume $150\mu m$ pitch for parallel strips in the outer barrel, with $100\mu m$ pitch in the rest of the detector. This assumption is convenient because it means that the parallel strips in the inner and outer barrel each occupy the same $\Delta\phi$.

The total number of channels per barrel shown in table 1 is about a factor of two larger than the estimate in the introduction. This was necessary because the distribution of particles along the length of the detector is not uniform, and because single particles can hit more than one strip — a serious problem for strips perpendicular to the beam.

The particle distributions in the simulations all come from Fritiof³. These simulations were done for p+p, p+Au, and Au+Au collisions assuming 100GeV/nucleon beams. The average charged particle multiplicities from these calculations are shown in table 2. The vertex position was assumed to always be on the central axis of the vertex detector. The z position was varied assuming a Gaussian distribution whose tails were cut off so that all interactions were assumed to take place within $\pm 50cm$ of the center of the vertex detector. The Gaussian distributions assumed⁶ $\sigma_z = 20, 16$, and $5.7cm$, for Au+Au, p+Au, and p+p collisions, respectively.

System	$\langle F \rangle$ = fraction of particles which hit detector	$\langle N_{total} \rangle$ No. charged particles
Au+Au (central)	0.64	5894
p+Au (min-bias)	0.55	50
p+p	0.56	21

Table 2: The average fraction of the particles which hit both layers of the vertex detector and the average total number of charged particles produced. Based on Fritiof³ for 100GeV/nucleon beams.

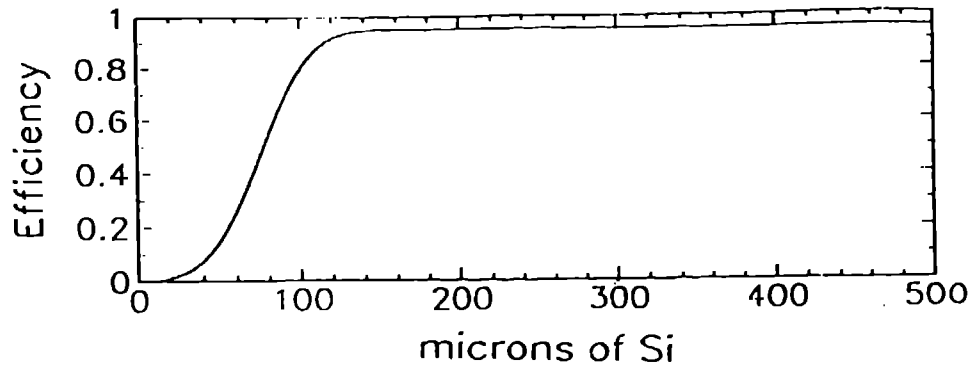


Figure 2: Assumed efficiency as a function of μm of Si traversed in a cell.

Each charged particle produced in the simulation was tested to see if it would hit the vertex detector; uncharged particles were ignored. If a particle entered the vertex detector, the program calculated which parallel and perpendicular strips would be hit. Multiple scattering of charged particles in the inner barrel of the vertex detector was included. To approximately account for the support structure and electronics, the multiple scattering calculation assumed that the inner barrel of the vertex detector was twice its real thickness. Particles were allowed to hit more than one strip. When a particle hit a detector barrel, the program calculated how much silicon a particle would pass through in each strip of the detector. A minimum-ionizing particle (*mip*) will lose an average of 116 keV in $300\mu m$ of Si. The result of this was an array giving the amount of Si (approximately equivalent to the energy loss) that particles passed through in a strip.

The array giving the amount of Si traversed in each strip is used to generate a pattern of "hits" in the strips. This is done using the efficiency function shown in fig. 2, which shows the efficiency as a function of the amount of Si traversed in a strip. The maximum efficiency⁶ was assumed to be 95%. A "threshold", corresponding to $\frac{1}{4}mip$ (or $75\mu m$ of Si here) was assumed. A noise level, which was varied from 0.1% to 0.01% was included in the efficiency function --- this means that a strip which was not hit has a small probability (P_{noise}) to be "on". If a strip was "on" then each of the adjacent strips were assumed to have a 10% probability to be "on" too --- introducing some charge sharing effects into the simulation. This final array holds the pattern of strips that were "on" or "off"

no analog information is used in the analysis of the events. The array was then used as input to algorithms to find the vertex, $dN/d\eta$, and the multiplicity.

The inner barrel has a "radius" of $R_1 = 6.1cm$, constrained by the beam pipe radius of 5 cm. If η is to be measured out to ± 3 , the length of the detector must be $\geq 4 R_1 / \tan(6^\circ) = 158cm$. A length of 50 cm has been chosen. The

variation in the vertex position means that for some events the coverage will extend above (below) $\eta = 3$ in the forward direction with a compensating decrease (increase) in the coverage around $\eta = -3$. The “radius” of the outer barrel is $R_2 = 1.5 \times R_1 = 9.2\text{cm}$.

In the following sections some discussion of the loss in performance expected from a modified design has been included along with the discussion of the detector described above. In these discussions, the conceptual design described here is compared to the vertex detector described in the Tales/Sparhc Letter of Intent⁷, which covers only $1/3$ of the azimuthal angle with strips perpendicular to the beam and is 64cm long instead of 100cm.

3 The problem of the angle of incidence

Particles entering the detector far from the vertex have incident angles nearly parallel ($\approx 7^\circ$) to the surface of the vertex detector. Consequently, a single particle will pass through many strips if the strips are oriented perpendicular to the beam axis. The number of hit strips as a function of z is $N_{strips} \approx (300\mu m \times z)/(100\mu m \times R) \approx 3 \times z/R$,

where z is the distance from the vertex and R is the radius of the barrel. At the ends of the detector, about 25 strips are hit in the inner barrel, for discriminator thresholds at $\frac{1}{4}mip$, as in E789 at Fermilab⁶. This threshold represents the highest threshold for full efficiency for normally incident particles; Landau fluctuations allow the energy loss in $300\mu m$ of Si to be as small as $1/2$ of the average energy loss. If this signal is split equally between two strips, then the signal in each will be $1/4$ of the mean. Particles incident nearly parallel to the surface would give about $1/3$ of the signal ($\approx \frac{1}{3}mip$) expected from a particle at normal incidence ($\approx 1mip$). So all 25 strips could register hits — drastically increasing the apparent occupancy. Realistically, considering Landau fluctuations in the energy loss in a thin layer, a threshold at $\frac{1}{4}mip$, compared to a signal of about $\frac{1}{3}mip$ would probably give some strips which would be “on” and some which would be “off”. This situation would make accurate measurements of the multiplicity and $dN/d\eta$ extremely difficult.

One solution to this problem is to turn the strips parallel to the beam direction. In this case, a particle at a nearly parallel incidence angle would give a large signal ($\approx 10mip$), essentially all in one strip. This eases the measurements of $dN/d\eta$ and multiplicity, but increases the dynamic range needed in the electronics.

4 Analysis of Monte Carlo Events: Multiplicity

The total multiplicity (N_{total}) and the detected multiplicity (N_{meas}) are related via $\langle N_{meas} \rangle = F \langle N_{total} \rangle$, or $N_{total} \approx N_{meas}/F$, where F and N_{total} are given in table 2. The uncertainty on N_{total} due to statistical fluctuations⁸ in the number of particles in the detector is:

$$\frac{\sigma_{total}}{N_{total}} \approx \sqrt{\frac{1-F}{(N_{total})F}} \quad (1)$$

Using the numbers in table 2 with eq. 1 allows the value of σ_{total}/N_{total} to be estimated as 1%, 13%, and 19% for Au+Au (central), p+Au (min-bias), and p+p, respectively. These fluctuations in the fraction of the particles detected set limits on the performance of the detector as an event-by-event multiplicity detector.

The performance of the detector will introduce further uncertainties in the multiplicity measurement. The important factors included in the simulations which affect the multiplicity measurement are the efficiency of the individual strips (see fig. 2), noise, the number of strips “hit” by a single particle, and multiple hits on a single strip. However, corrections for all of these effects can be made.

When⁶ $P_{noise} = 10^{-3}$, the average number of hits due to noise in the parallel strips will be 38.4 per barrel. This is not an important correction for central Au+Au collisions, but is significant for p+p and p+Au. In these cases, this (pessimistic) noise level is frequently greater than the number of real hits in the inner barrel. Therefore, it will be important to both minimize and understand the noise in the detector.

Eq. 1 gives an estimate of the loss in performance from a reduction in the coverage of the vertex detector. Given the large multiplicity in a central Au+Au collision, a slightly smaller detector would give a good measurement of the multiplicity. However, the reduced coverage of the vertex detector described in the Tales/Sparhc letter of intent⁷ would further degrade the already marginal accuracy of the p+p and p+Au multiplicity measurements. Although the solid angle coverage of such a detector would be sufficient to measure the multiplicity for central Au+Au collisions, its use of parallel alone strips could complicate the measurement.

5 Analysis of Monte Carlo Events: $dN/d\eta$

The problems associated with the $dN/d\eta$ measurement are similar to those of the multiplicity measurement. The major additional complication is the

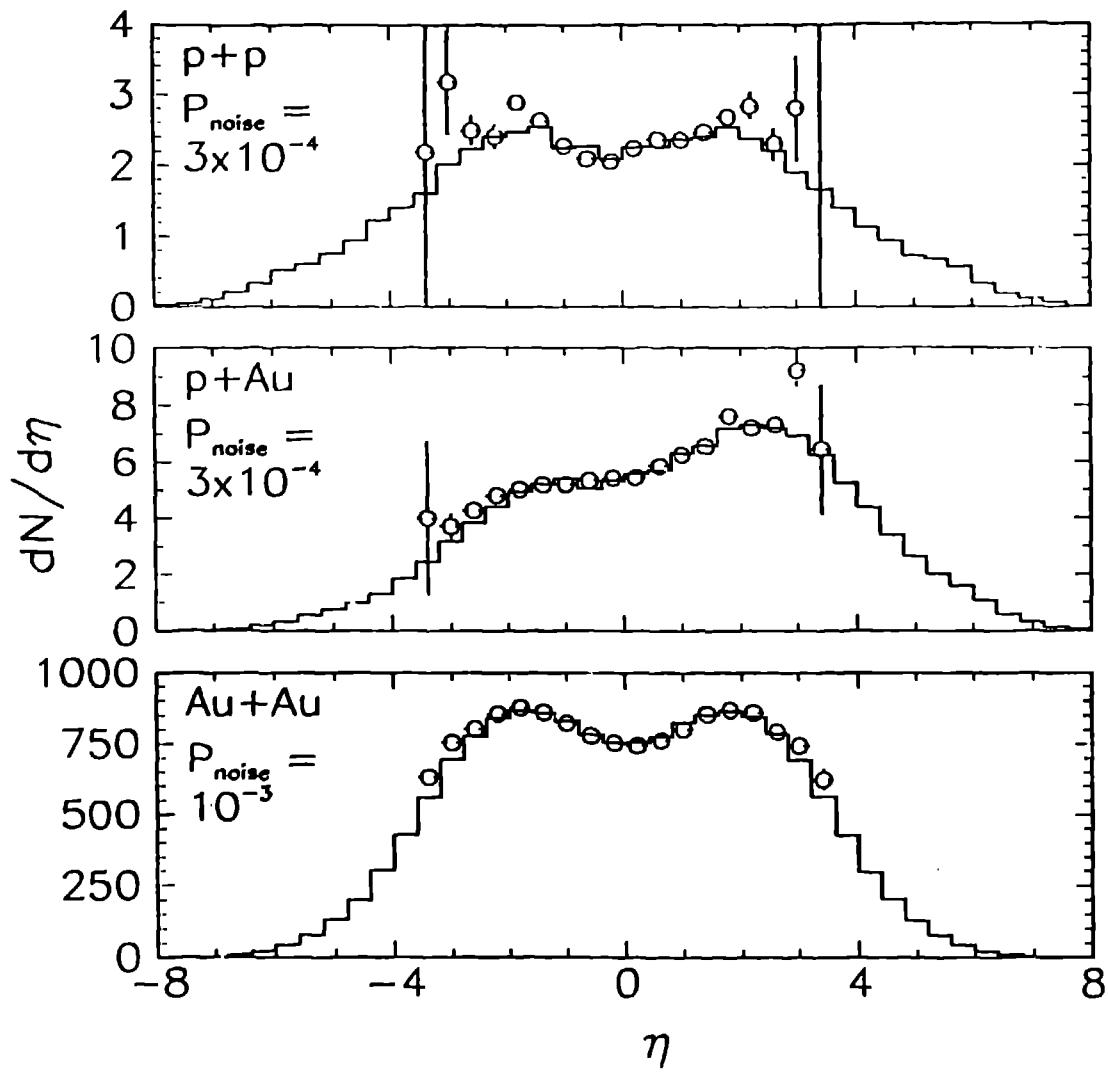


Figure 3: “Real” (histogram) and measured $dN/d\eta$ distributions (circles with error bars) for p+p, p+Au, and Au+Au. Only the inner barrel was used to get “measured” distributions. $P_{\text{noise}} = 3 \times 10^{-4}$ was assumed for p+p and p+Au.

determination of the vertex to allow calculation of the pseudo-rapidity ($\eta = -\ln(\tan(\frac{\theta}{2}))$). $dN/d\eta$ measurements are generally averages for many events. Statistical fluctuations in the average over many events are therefore less important than the event-by-event fluctuations in the total multiplicity. Consequently, $dN/d\eta$ measurements should be possible for p+p, p+Au, and Au+Au.

First, the vertex position must be found, this is discussed in the following section. Next, the range of η occupied by each chip is calculated. Because the chips with strips parallel to the beam give more reliable information on the number of hits, only those are used to calculate the number of hits (N_{hit}) in each range of η . Corrections for the efficiency, noise, double hits, and charge sharing are made. The “measured” $dN/d\eta$ value is the average of $N_{hit}/\Delta\eta$ over many events.

Fig. 3 compares the “real” and “measured” $dN/d\eta$ distributions for p+p, p+Au, and Au+Au events. The shapes of the “measured” distributions are always close to the “real” distributions. Since the distributions are calculated using the vertex found by the pseudo-tracking algorithm, which does not always find the correct vertex, some of the differences may be from events with an incorrect vertex position used in the calculation.

As with the multiplicity measurements, noise complicates the $dN/d\eta$ measurements. The number of particles which hit each chip is much smaller near the edges of the detector, but noise causes a constant fraction of the strips to be “on”. This means that the signal/noise ratio is much worse (factor of ≈ 10) at the largest $|\eta|$ values. For p+Au, even with the optimistic assumption that $P_{noise} = 10^{-4}$, the signal and noise will be comparable around $\eta = \pm 3$, resulting in larger statistical uncertainties on the points around these η values. This noise problem will be worse for p+p collisions where the multiplicity is lower, but unimportant for central Au+Au events.

6 Analysis of Monte Carlo Events: Vertex Finding

The vertex detector must also be able to find the vertex. As an aid in understanding this process, figs. 4-5 show the number of hits on the vertex detector vs. z for a p+p event and for a Au+Au event. Hits on the parallel strips (left side) and perpendicular strips (right side) and on the inner barrel (top) and outer barrel (bottom) are shown separately. For perpendicular strips the number of clusters of adjacent hits vs. z is shown — not the raw number of hits. The real vertex positions are marked. By looking at these figures, it is clear that the distribution of hits on the parallel strips can be used to estimate the vertex position for Au+Au, but for p+p the small number of hits, coupled with the noise, makes it difficult to find the vertex from this information alone.

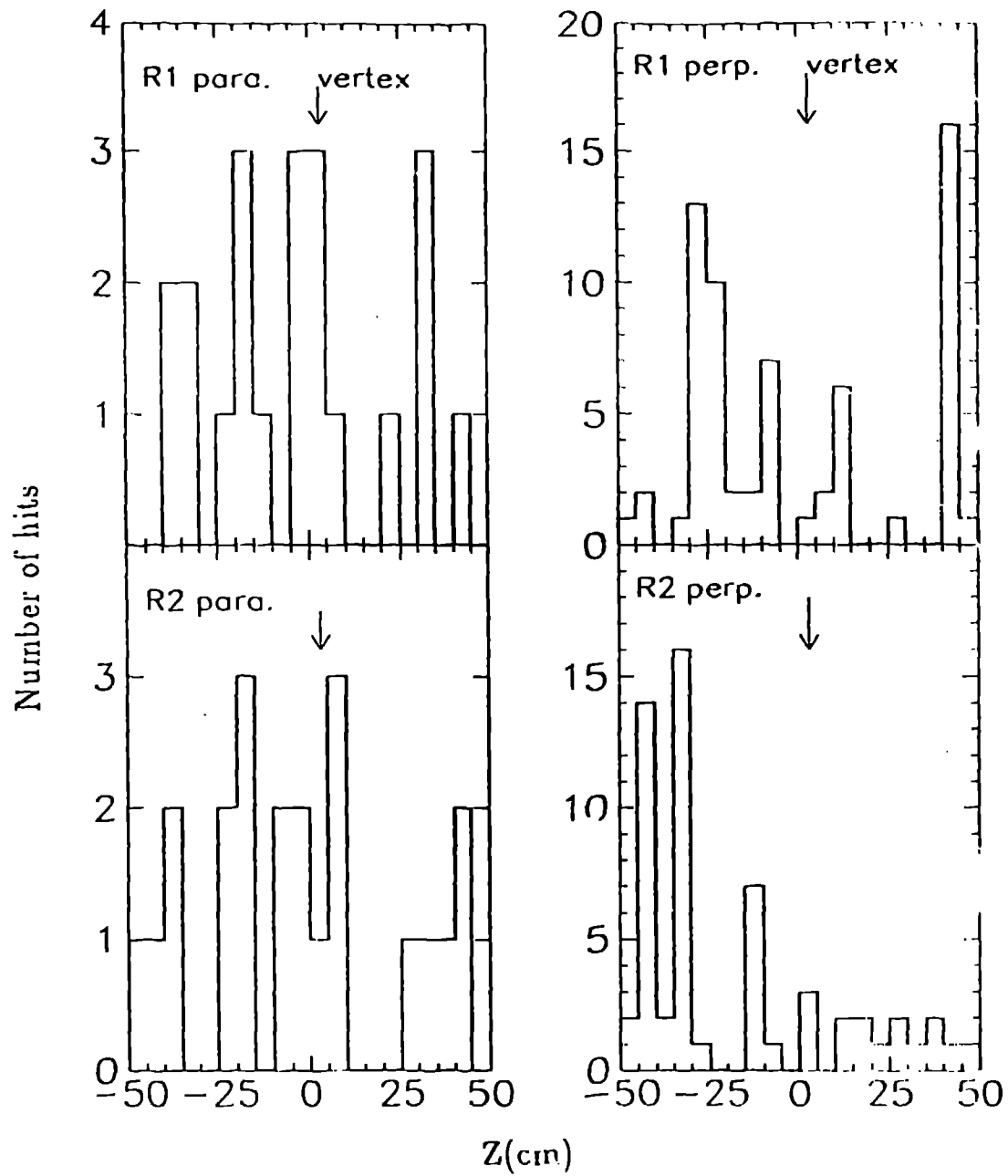


Figure 4: $p+p$ - a sample event. The left side shows the number of hits vs. z (the beam direction) for parallel strips. The right side shows the number of hits vs. z for perpendicular strips. The top half shows hits on the inner barrel (R1) and the bottom half shows hits on the outer barrel (R2). The arrows mark the vertex position.

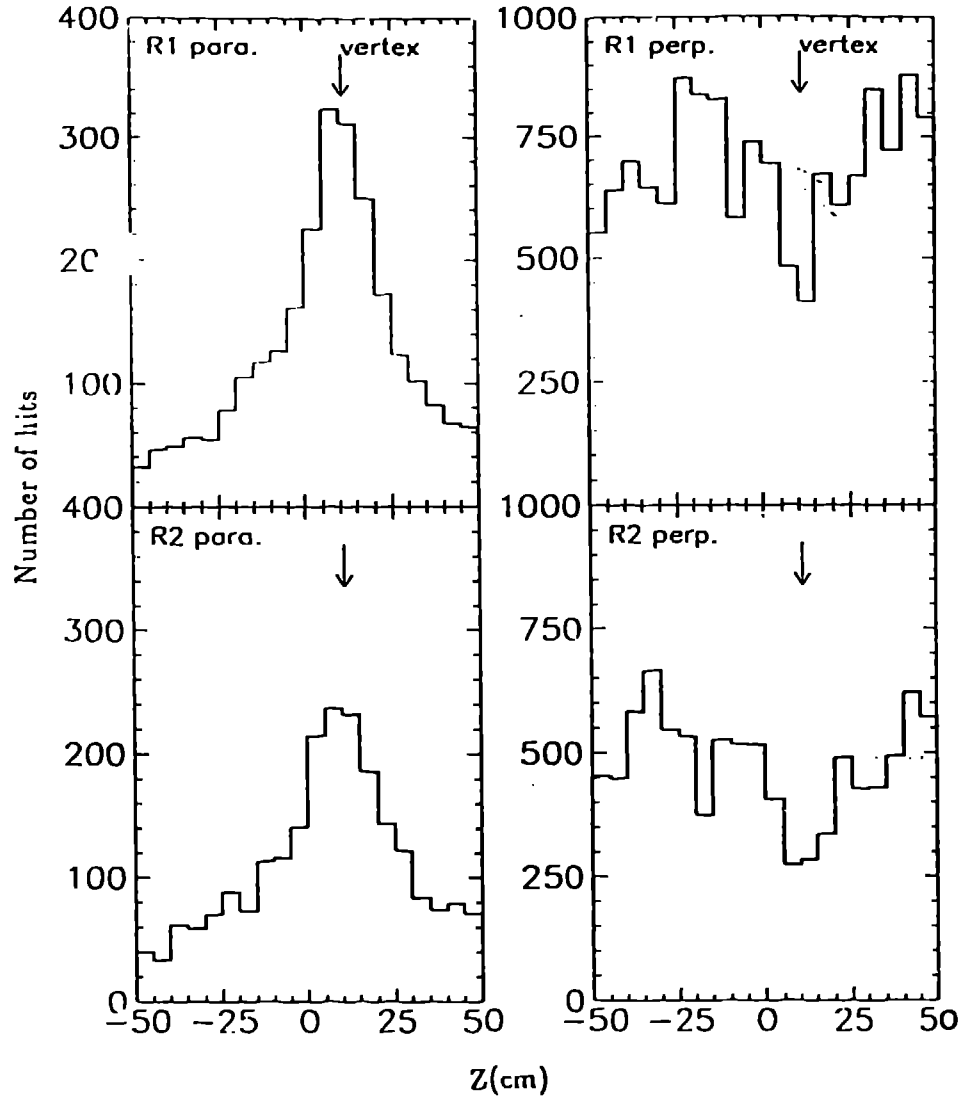


Figure 5: $\text{Au}+\text{Au}$ - a sample event. The left side shows the number of hits vs. z (the beam direction) for parallel strips. The right side shows the number of hits vs. z for perpendicular strips. The top half shows hits on the inner barrel (R1) and the bottom half shows hits on the outer barrel (R2). The arrows mark the vertex position.

6.1 Vertex from Center of Gravity

The simplest algorithm to find the vertex in a symmetric collision would be to find the center of gravity (CG) of all hits. It is not clear how well this should work in the asymmetric case of p+Au. However, by taking the difference between the CG in the inner and outer barrels, it could be possible to project towards the vertex in this case. Information from parallel strips only was used to find the vertex from the CG, using two iterations. First, the whole hits distribution (see the left sides of figures 4-5) was used. Then an equal number of channels above and below this initial CG were used to improve the vertex position measurement.

There is a statistical limit to this method. The minimum uncertainty on the vertex position is $\approx(\text{rms width})/\sqrt{N} \approx 0.4\text{cm}$ for central Au+Au collisions, which is below the vertex resolution required at the trigger level ($\approx 1\text{cm}$), but insufficient for the offline analysis ($\approx 1\text{mm}$). The actual vertex resolution found using the CG method was $\sigma=2.1\text{cm}$ for Au+Au. For p+p and p+Au, the number of hits on the vertex detector is much smaller and the statistics do not allow a sufficiently accurate estimate of the vertex position using the CG only, especially when random hits due to noise are included.

6.2 Vertex from Pseudo-tracking

Another method used to find the vertex is based on "pseudo-tracking." This method treats all pairs of hits in the inner and outer barrels as potential tracks and calculates a vertex position from them. The real vertex appears as the most probable value of the vertex position.

There are two stages in the pseudo-tracking vertex search. First, only the parallel strips are used, obviating the need to test all pairs of hits as each parallel strip covers a small $\Delta\phi$ (azimuthal angle). Particles from the central axis of the vertex detector have the same ϕ at each barrel, except for small variations due to multiple scattering. Fig. 6 shows a distribution of the change in the strip number hit in the outer barrel due to multiple scattering in the inner barrel; most particles hit the outer barrel within ± 2 strips of the expected position. For each hit in the outer barrel, all hits in the inner barrel which are within ± 2 strips are used to calculate a possible vertex position. The top part of fig. 7 shows the resulting distribution of vertices for a sample Au+Au event. An estimate of the event vertex appears as a peak. The peak height gives the number of particles hitting both barrels of this half of the detector. The background comes from random pairs of hits. Limiting the hits tested to ± 2 strips reduces the number of pairs that must be tested by a factor of $\approx \frac{56095}{640 \times 3} = \frac{1}{361}$. This reduces the background in the histograms shown in the upper half of fig. 7 by $\frac{1}{361}$ while only reducing the counts in the peak by about 12% (see fig. 6).

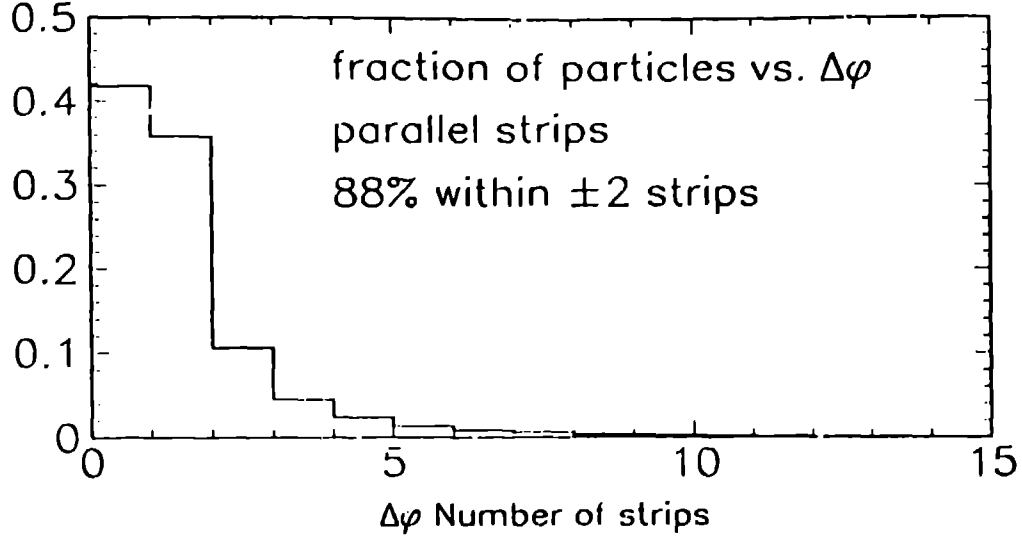


Figure 6: Probability vs. the difference in the parallel strip in the outer barrel which was hit and the strip that would have been hit with no multiple scattering. All charged particles which hit both barrels are included.

Because the peak found using pseudo-tracking with parallel strips is broad, the vertex position is estimated by taking the center of gravity of three bins around the maximum. Because the strips are long (5cm) in the z direction, this method can not give very good vertex resolution. Fig. 8 shows the vertex resolution for p+p, p+Au, and Au+Au using pseudo-tracking with parallel strips only. For p+p and p+Au, this method gives better resolution than the center of (CG) and is much less noise sensitive. However, pseudo-tracking with parallel strips alone still does not give a vertex resolution for p+p which is significantly better than the variation in the vertex position itself⁶.

This first stage using parallel strips is used to estimate a vertex position. The second stage of the vertex search uses perpendicular strips which are short in the z direction ($100\mu\text{m}$), and determine the vertex much more accurately. Beginning with an approximate vertex reduces the range of vertex positions to be searched and increases the speed of the algorithm. The second stage of the vertex search is similar to the first, but as each perpendicular strip occupies a large $\Delta\phi$, the number of pairs of hits that must be tested is about $N_1 N_2 / 3$, where 3 is the number of different azimuthal segments with perpendicular strips and N_1 and N_2 are the number of hits on the perpendicular strips in the inner and outer barrels, respectively. For central Au+Au events, this number is large, so the algorithm is slow. The vertex from the first stage of pseudo tracking is used to restrict the pairs of strips which are tested; for Au+Au, only those pairs of strips which point to a vertex position within $\pm 5\text{cm}$ of the vertex found in

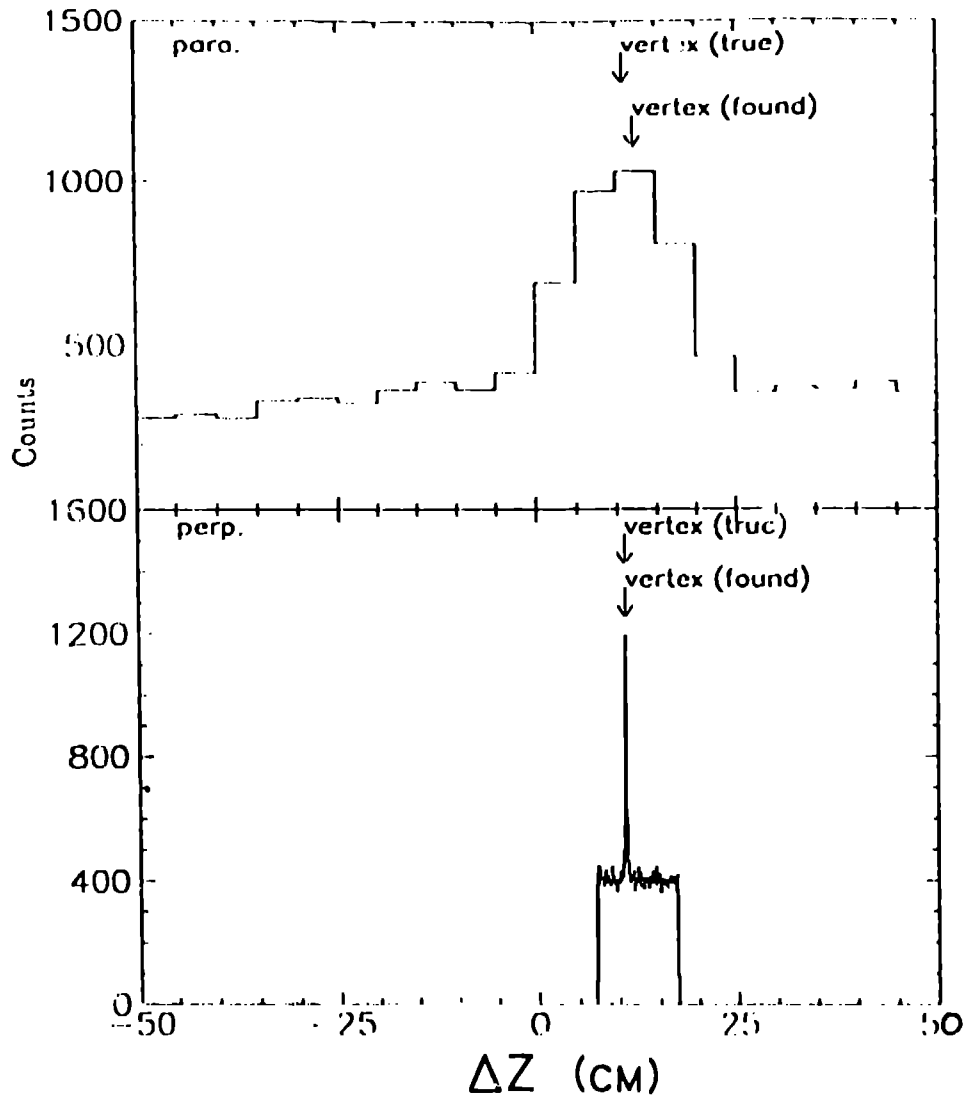


Figure 7: Au+Au pseudo-tracking example. Top shows the distribution of vertices using parallel strips only. Bottom shows the distribution of vertices using the perpendicular strips. Arrows mark the true vertex and the vertex found in each stage.

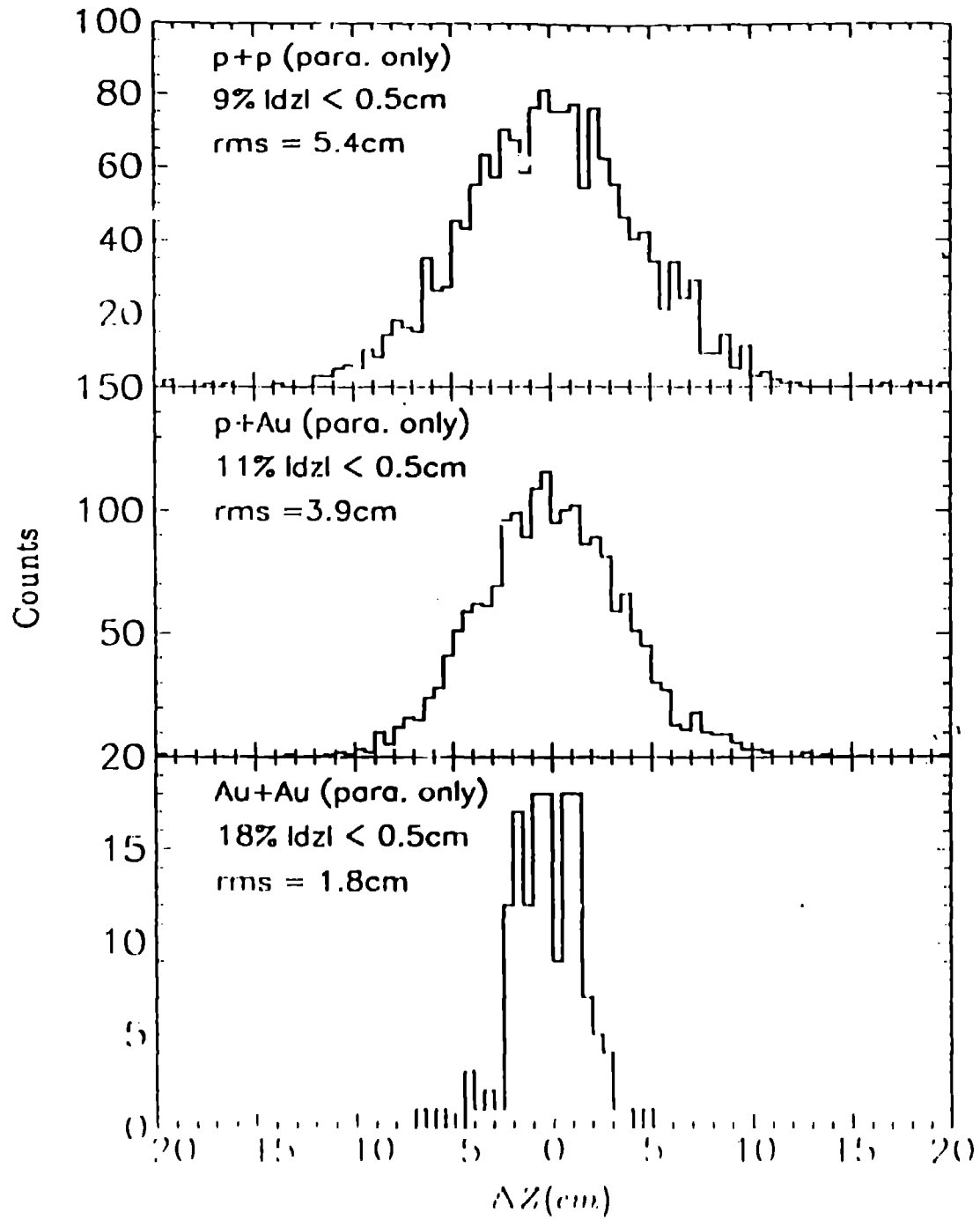


Figure 8: The vertex resolution using pseudo tracking with parallel strips only for p+p, p+Au minimum bias, and Au+Au central. The horizontal axis is the difference the true vertex and the vertex found.

the first stage of pseudo-tracking are tested. For p+p and p+Au, this range is expanded to $\pm 10\text{cm}$. A histogram of vertex positions is calculated from the pairs of hits. An example of one of these histograms is shown on the bottom part of fig. 7. The vertex position appears as the peak in this distribution.

Fig. 9 shows the vertex resolution using both stages of pseudo-tracking. The correct vertex is found in all events tested for central Au+Au collisions. For p+p and Au+Au the correct vertex is usually found. Table 3 summarizes the efficiency of pseudo-tracking vertex search for different assumed levels of noise for the three systems. "Total events" and "triggers" are the total number of Monte Carlo events and the number of those that satisfied the "trigger" condition — at least two charged particles hitting both cylinders of the vertex detector. The column labeled "% of triggers" gives the efficiency of the vertex search algorithm — the fraction of the events for which the vertex found was within 5mm of the true vertex. The last column gives the resolution of the vertex finding algorithm based on the widths of the peaks in fig. 9. These widths are upper limits due to the size of the bins used in the pseudo-tracking algorithm. Especially for p+p collisions, noise has a significant effect on the vertex finding efficiency.

system	P_{noise}	Total events	Triggers	% of triggers	σ (mm)
p+p	0.0001	2000	1699	91%	≤ 0.4
p+p	0.0003	2000	1699	86%	≤ 0.4
p+p	0.0010	2000	1699	71%	≤ 0.4
p+Au	0.0001	2000	1921	97%	≤ 0.3
p+Au	0.0003	2000	1921	94%	≤ 0.3
p+Au	0.0010	2000	1921	90%	≤ 0.3
Au+Au	0.001	150	150	100%	≤ 0.2

Table 3: Efficiency of pseudo-tracking vertex search vs. assumed level of noise for p+p, p+Au, Au+Au. Interaction diamond assumes $\sigma_I = 5, 7, 16, 20\text{cm}$ for p+p, p+Au, Au+Au, respectively. See text for explanation of columns.

Fig. 10 demonstrates one source of problems with the pseudo-tracking vertex search — when the multiplicity is very low, the probability of finding the vertex is also low and this probability gets smaller for higher noise levels. Higher noise levels have a significant effect on the vertex finding efficiency at low multiplicity (below ≈ 10), but the efficiency reaches $\approx 100\%$ in each case for sufficiently high multiplicity. In an ideal case, with no noise, 100% efficiency, and no multiple scattering, the algorithm would work for even one charged particle hitting both layers of the detector.

A vertex detector like the one described in the Taley/Sparke letter of intent

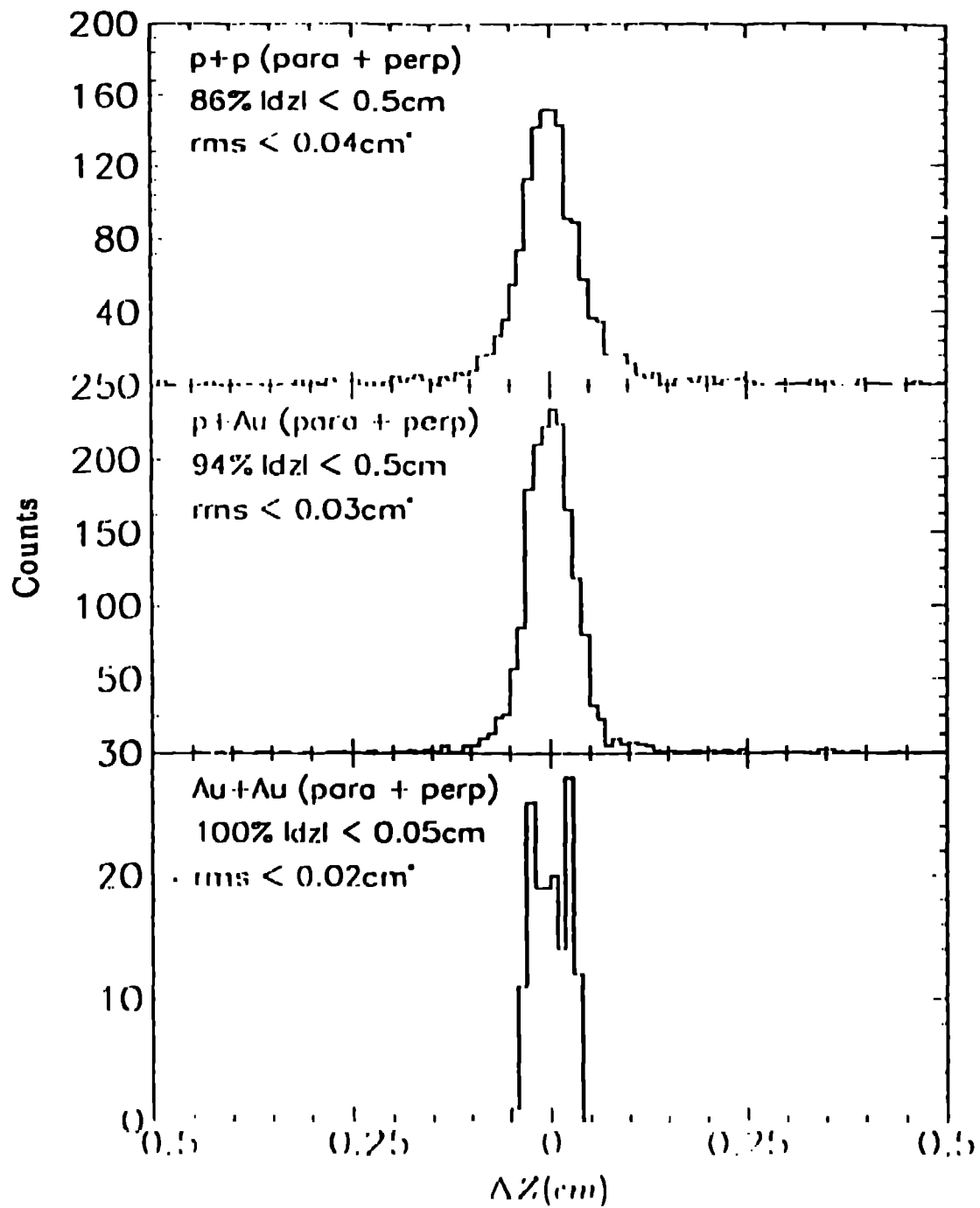


Figure 9: Notice the difference in scale from fig. 8. The vertex resolution using pseudo tracking with both parallel and perpendicular strips for p+p, p+Au minimum bias, and Au+Au central. * Due to the bin size used, the RMS deviations are upper limits.

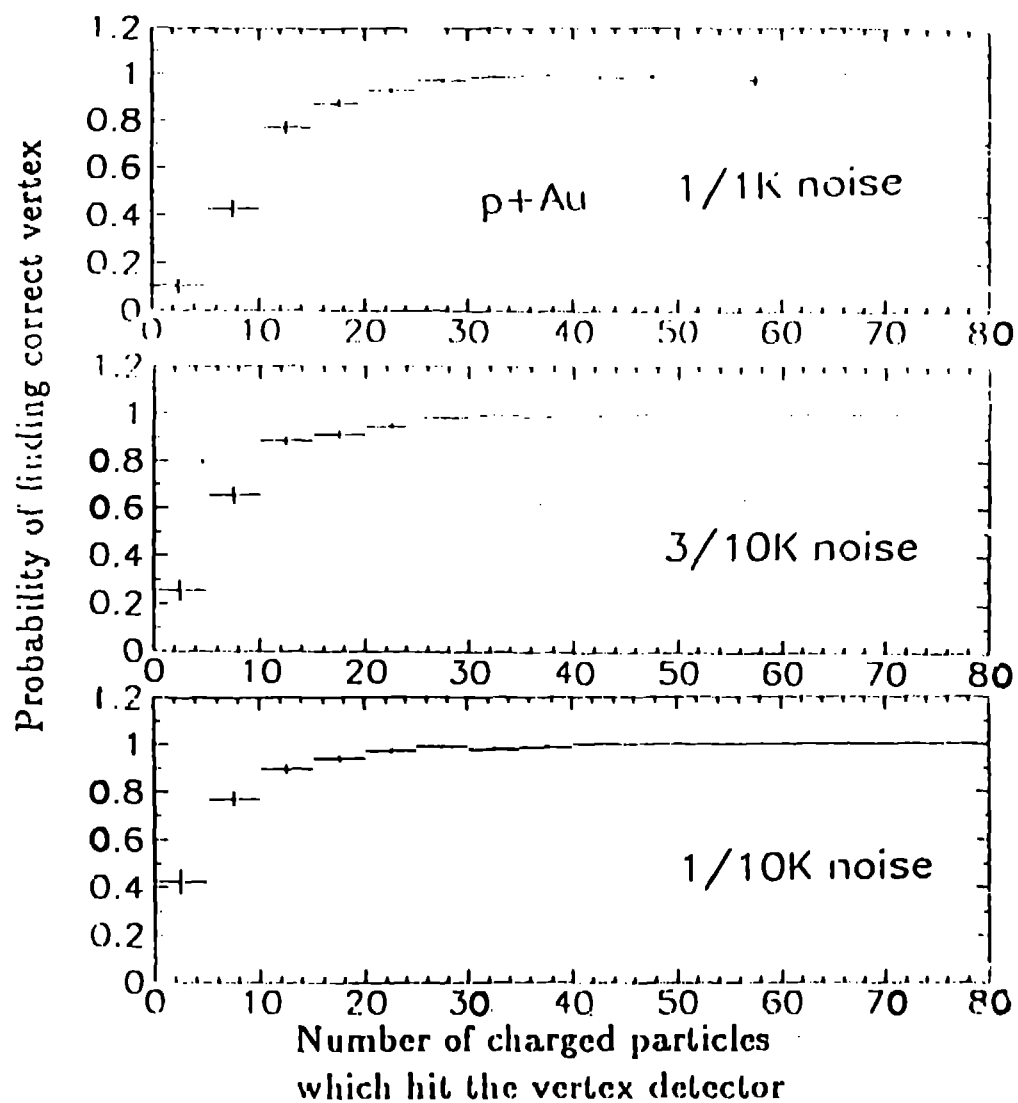


Figure 10: p+Au minimum-bias events from *Fritiof*. The probability that the correct vertex will be found vs. the number of charged particles that hit both layers of the vertex detector for three assumptions about the noise level. Note the differences in efficiency for the lowest multiplicity, where the effects of noise are most important.

system	P_{noise}	Total events	Triggers	Vertex correct	% of Triggers
p+p	0.0003	2000	1699	1228	72%
p+Au	0.0003	2000	1921	1662	87%
Au+Au	0.001	150	150	150	100%

Table 4: Efficiency of pseudo-tracking vertex search for p+p, p+Au, Au+Au with only 2 azimuthal segments of perpendicular strips used and a length of 64cm. Interaction diamond assumes $\sigma_I = 5.7, 16, 20\text{cm}$ for p+p, p+Au, Au+Au, respectively. Compare this to table 4, using the full detector.

which had only 2 azimuthal segments of strips perpendicular to the beam, instead of 3, and was 64 cm long, instead of 100cm, could still find the vertex, but with reduced efficiency. Table 4 shows the expected vertex finding efficiency for this detector configuration. The efficiencies are smaller (compare to table 3), especially for p+p, but if the cost savings are large enough, the efficiency loss may be acceptable. Some efficiency is lost when the vertex is outside the shorter detector. However, tests with the full detector configuration show that the pseudo-tracking algorithm can find the vertex in central Au+Au collisions in 94 out of 100 events even when it is 50cm outside of the detector (100cm from the center of the detector), although the resolution falls to $\sigma \approx 2\text{mm}$.

6.3 Vertex from the Correlation Method

The most interesting of the vertex finding methods tested here is based on correlations between the pattern of hits on the inner and outer detectors. This method uses a single row of chips on the inner barrel and the corresponding coverage on the outer barrel, or 1/6th of the total circumference.

When an interaction occurs, tracks project outward from the vertex, producing a pattern of hit strips on the inner and outer barrel. To first order, the pattern on the outer barrel is equal to that on the inner barrel except that all distances between hit strips are increased by a factor of (R_2/R_1) . If we take the pattern on the outer barrel, and shrink it by a factor of R_1/R_2 , we would be able to take this new pattern, and slide it along the inner barrel until there is a perfect match between the hit patterns on the two barrels. We search for the match by forming the correlation function between the patterns as a function of relative position z . For any z we multiply ("and" in hardware) the value of the strip on the inner barrel (1 = hit, 0 = no hit) by the value of the overlying strip of the outer barrel, and sum these values for all strips. For a randomly chosen relative offset this sum will be small (to first order equal to the multiplicity in the segment of the outer barrel tested times the occupancy of the inner barrel), but when the patterns match, the sum will be equal to the multiplicity in the

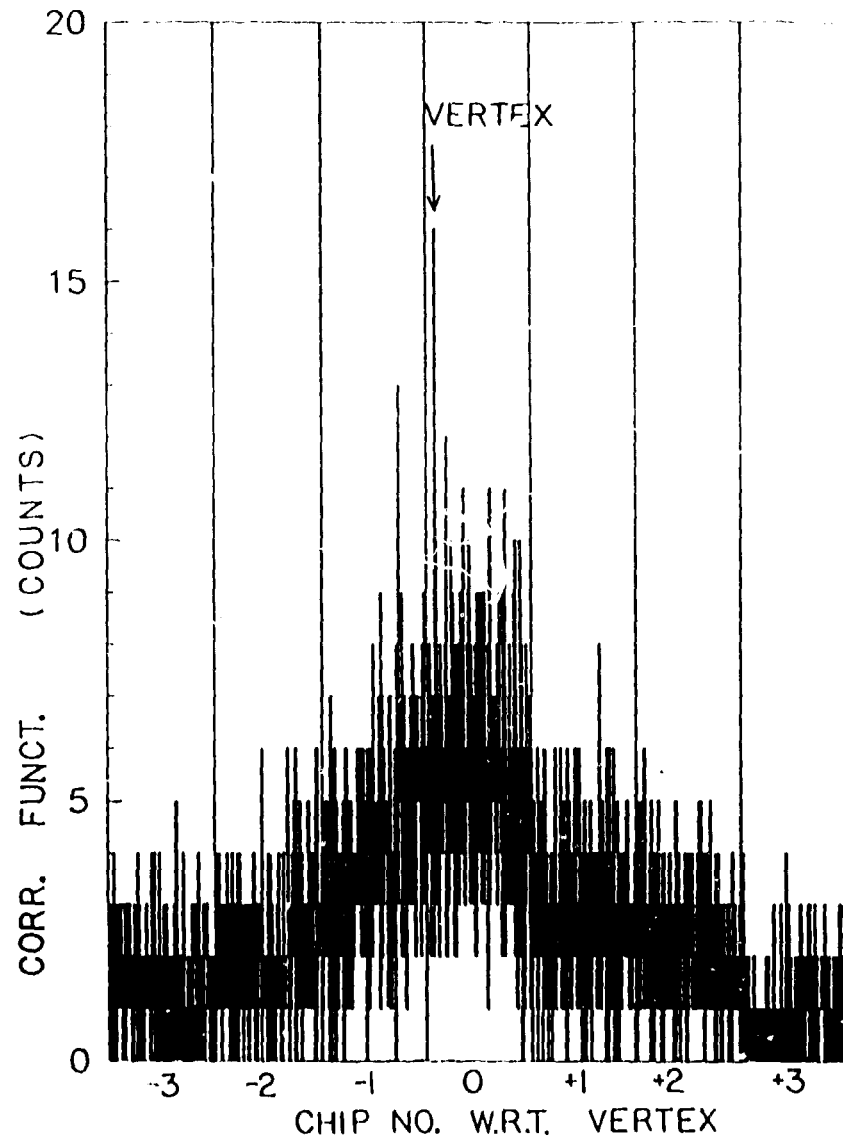


Figure 11: Correlation function for 7 adjacent chips in the vicinity of the vertex. Realistic case — multiple strips turned “on” by slanting tracks, multiple scattering on, $R2/R1 = 1.5$. The peak now occupies more than one channel, but it is still easily found.

ideal case. The value of z in this case translates directly into the event vertex position with a resolution equal to one strip width.

A hardware implementation to deliver this vertex position would execute the calculation described above on each pair of inner/outer chips in parallel. Thus one of the 20 pairs finds the vertex, all others turn up null answers. This algorithm works for central Au+Au events, but for the lower multiplicities of p+p and p+Au collisions, there are not enough hits per chip to reliably find the vertex. However, offline the algorithm could be extended to use all hits in all chips, and the method would also work for p+Au and p+p collisions. In this limit the algorithm's efficiency would be similar to that of pseudo-tracking.

A series of tests were done for $R_1 = 6\text{cm}$ and $R_2 = 12\text{cm}$. Using central Au+Au events for the ideal case where each track turns on only one strip and ignoring multiple scattering, the algorithm finds the correct vertex in 20/20 events with a (peak)/(average background) ratio of about 3/1. Allowing each track to turn on multiple strips due to its angle of incidence increases the apparent occupancy far from the vertex, and the algorithm never finds the vertex in this case. However, when clusters of contiguous hits were replaced by a single hit, the algorithm finds the vertex in 20/20 cases again, still assuming no multiple scattering. The peak/background ratio remained around 3/1. Including multiple scattering spreads hits across neighboring strips, and reduces the signal without changing the background. In this case the algorithm found the correct vertex 17/20 times with a typical (peak)/(average background) ratio of about 2/1. The last step was to reduce the radius of the outer barrel to $R_2 = 1.5R_1$, which matches the current detector design. This reduces the effect of multiple scattering, and the correct vertex is found in 19/20 cases with a typical (peak)/(average background) ratio slightly larger than 2. An example of the resulting correlation function is shown in fig. 11, for 7 chips centered on the chip over the vertex. The channel corresponding to the vertex appears as the maximum value. Increasing the number of adjacent channels used to calculate the correlation function would improve the peak to background ratio.

The correlation method is much faster than the pseudo-tracking method. However, because it requires the patterns of hits to line up exactly in the two barrels, it is more sensitive to multiple scattering than the pseudo-tracking method. The on-line version of the correlation method requires at least a few tracks going into the chip over the vertex, which does not generally happen for p+p and p+Au events. The offline version of the correlation method, using all strips, found the correct vertex in 18/20 events for p+Au, which is similar to the efficiency of the pseudo-tracking method.

7 Alignment requirements

We have assumed that the vertex needs to be known to better than 1mm in z . In the plane transverse to the beam, the definition is already equal to the beam size ($\sigma_T \approx 0.45\text{mm}$ for Au+Au^{5,9}). Some chip placement aberrations result in a track ending up in a strip neighboring the expected one, reducing the peak value of the correlation function. Preventing this kind of error defines most of the constraints on placement of the chips in 3 directions, z (along the beam axis), R (radial), and s (circumferential, or $R \cdot d\phi$), plus the 3 rotations around these axes. The chips lie at radii R_1 and R_2 , which are assumed to be 6 and 9 cm in the calculations below. The size of a chip in the z -direction (Z_{chip}) is taken to be 5cm, and the detector “cylinders” have a hexagonal cross-section.

The correlation method is only concerned with the relative placement of chip pairs, one chip on the inner cylinder and the corresponding chip(s) on the outer cylinder. Here, one example of the determination of the alignment constraints is given. The other constraints are determined similarly and are summarized in table 5.

Consider the displacement in R (ΔR) of one of the cylinders relative to the other. When scaling the outer pattern by the nominal R_1/R_2 , a radial displacement would result in a pattern that is improperly scaled. A calibration procedure could find the actual R_1/R_2 , but the nominal ratio will presumably be a ratio of integers, hard-wired in a fast vertex finder. In order to limit the error such that in the worst case, a track is displaced by 1 strip ($100\mu\text{m}$),

$$100\mu\text{m} = \frac{R_1}{R_2} \times \frac{Z_{chip}}{R_2} \times \Delta R \quad (2)$$

This is satisfied if radial displacement of the outer chip is less than $\approx 0.3\text{mm}$.

axis	max. error in relative position	max. error for relative rotation about this axis
z (beam)	0.5mm	0.15°
R (transverse)	0.3mm	0.1°
s (circumference)	0.5mm	0.3°

Table 5: Summary of tolerances in placement of inner/outer chip pairs relative to each other from correlation method

These tolerances, summarized in table 5, are between inner/outer chip pairs only. Suppose that a chip pair is joined such that they meet these tolerances. There are further constraints on the positions of chips pairs relative to the beam. Again, consider one example. There is a constraint in R , which leads to a limit of:

$$dR = \frac{R_2}{R_1} \cdot \frac{R_1}{R_2} \cdot \frac{Z_{chip}}{R_2} \cdot \frac{R_1}{R_2} = 100\mu\text{m}. \quad (3)$$

The pair must be placed at a radial distance which is known better than $dR \approx 0.8\text{mm}$. This should be compared to the size of the Au+Au beam in the transverse direction^{6,9}, $\sigma_T \approx 0.45\text{mm}$. Table 6 summarizes the constraints on the positions of pairs of chips relative to the beam. These constraints are not as stringent as those on the relative positions of the chips.

axis	max. error	max. error for rotation about this axis
z	5.0mm	1°
R	0.8mm	37°
s	∞	4°

Table 6: Summary of tolerances on the placement of chip pairs relative to the beam from correlation method, where each pair of chips are positioned relative to each other within the tolerances given in table 5.

The correlation method of vertex finding leads to the limits given in tables 5 and 6. The pseudo-tracking method combines a hit on any of the inside chips with a hit on any of the outer chips, which may pose limits on the relative placement of all chips simultaneously, not just in pairs. In order for this method to work, all pairs must be able to point to the same vertex. This implies relative placement requirements between any pairs of chips similar to those in table 5. However, this is an offline method, and the positions of chips may be calibrated using tracks reconstructed from other detectors. Such calibrations would work for all aberrations except rotations around r and z . However the tolerances imposed on these angular placements by the correlation method are much more stringent than anything needed to define a vertex to 1mm. Thus the pseudo-tracking method imposes no further restrictions.

8 Electronics Requirements

There are several important constraints on the design of the electronics for the vertex detector. The size and mass must be minimized to prevent space conflicts with other detectors and to minimize multiple scattering and production of secondary particles. The electronics system must produce as little heat as possible; if the power consumption can be kept to the order of $\approx 1\text{mW/channel}$, then forced-air cooling should be possible. If air cooling is not possible, a complicated and potentially expensive cooling system will be required, which would add significant mass in the vertex region. The shaping time of the preamplifier must allow individual beam crossings (every $\approx 200\text{ns}$) to be distinguished. Since the vertex detector multiplicity is expected to form part of the first level trigger, a system which moves this information “into the pipeline” at this rate is

needed. This time constraint, combined with the power consumption constraint eliminates most of the presently available electronics components.

There are several Si strip vertex detectors currently being designed (for instance for GEM and SDC at the SSC), and some already in operation^{6,10-15}. As a result, some components are available. However, none of these components can be considered completely "off-the-shelf" items. Even in those cases where a similar component has been made before, some modifications will be necessary. For example, the Si strip detector wafers similar to the ones needed for this detector have been constructed by a number of vendors¹⁶⁻²⁰. However, in order to purchase them for use with this detector, a new set of masks must be made for the appropriate strip pitch and length. Then the detectors must be manufactured and tested. Quality control is time-consuming, but vital, as is working closely with the vendors. A well-defined and complete set of quality-control parameters must be agreed upon with the vendor. For a project of this scale, automated testing on a probe station will probably be necessary. A custom probe card and some of the related software would have to be provided. Our experience suggests that this process typically takes ≈ 18 months (or more) before all of the detector elements are in hand.

The first part of the electronics system is the connection of the detector strip to the preamplifier. Although some work is being done to integrate the front-end electronics and the detector strips^{19,20} on a single wafer, we expect to have a separate front-end integrated-circuit chip which will be wire-bonded to the detector strips. Here, the $100\mu\text{m}$ pitch is advantageous since machines exist for wire-bonding at this pitch. The front-end electronics chip would consist of a preamplifier, shaper, discriminator, and latch. An LED-based optical fiber readout system, for high speed ($\approx 100\text{MHz}$) and low local power consumption will probably be used. In order to simplify the mechanical design, the electronics packages would be supported on the Si detector chips.

The simulations have shown that it is possible to satisfy all of the vertex detector's design criteria without using ADC's on the individual strips. This would simplify the system and reduce the volume of data produced. However, a single analog output for each detector chip would be useful for triggering. Due to the angle of incidence problems, a simple sum of the analog signals from each chip would not give the multiplicity without first determining the vertex position. For a multiplicity to be used in the trigger, a sum of discriminator outputs from the strips parallel to the beam (where ≈ 1 strip per particle would be "hit") is needed. A sum of the analog signals from all strips on a chip might be useful; if $dN/d\eta$ is constant over the length of the vertex detector (based on Fritiof calculation, this is true at the $\approx 15\%$ level — see fig. 3), then the total energy loss in each detector would be proportional to $dN/d\eta$ independent of the z position relative to the vertex. This is similar to an observation in the Oasis Letter of Intent²¹, although that vertex detector geometry was much

Source	Description	Available now?	Where used or to be used	Approx. peaking time (ns)	Power use (mW/chan)
FNAL ^{6,10}	bipolar	Yes	E789	10	≥ 50
LBL ^{11,24}	SVX-D: shaper, disc., latch., digital circuits, Some rad. damage problems	Yes	CDF (SVX-I)	≈ 700	$\approx 1-2$
FNAL/ORNL ²⁵	R&D: CMOS preamp, shaper prototype (now), more later	Yes*	BVX(D0), RHIC?	≈ 200	
LBL ²⁶	SVX-H: rad. hard CMOS, shaper, disc., latch, digital circuits	Yes*	CDF (SVX-II), L3	≈ 500	$\approx 1-2?$
LBL ²⁷	CMOS preamp, shaper, disc, latch, analog sum?, no buffering	No	SDC	15?	
Santa Cruz ²⁸		No	SDC		
Ikeda ¹⁹	R&D: combined Si strip detectors & front-end	Yes*	SDC		7
SDI ²⁰	R&D: BiCMOS combined Si strip detectors & front-end	No			

Table 7: Selected sources of front-end electronics for Si strips vertex detectors. The last two columns gives the approximate peaking time and power dissipation.

* indicates that only prototypes are available.

different. This quantity could also be useful in triggering. Knowing $dN/d\eta$ implies knowledge of the multiplicity only if the vertex position is known — so if the multiplicity is needed for the first level trigger, the need for parallel strips remains.

More work is needed to design, manufacture, and test suitable front-end electronics components. Some work on this subject has been reported at this conference^{22,23}. This important work should lead to front-end electronics systems which are fast enough and have low enough power consumption. A summary of selected electronics systems for Si strip detector appears in table 6. None of the currently available components satisfies the combined power dissipation and speed limitations for this detector. In addition, it is crucial to integrate the components into a system as soon as possible. It would be unwise to start construction of an expensive and complex detector system without careful tests of all of the components together. Some of this integration work is already being done by the P2 group in Los Alamos. Prototype CMOS preamplifiers²⁵ have been acquired and will be combined with an OPAL-type strip detector¹⁷, using a locally developed hybrid circuit. Tests of this system will take place in early 1992, with tests of other systems²⁶ following shortly.

The electronics development can take place using either CMOS or bipolar processes. CMOS circuits are easier and cheaper to develop, but are not suitable for long strips, which have large capacitance — this is not a limitation in the current design, but could be for other designs. It will be easier to develop circuits with less than $100\mu\text{m}$ pitch using a bipolar process than with CMOS — but the current design assumes $100\mu\text{m}$ — eliminating this advantage. In general, bipolar circuits use less power for the same performance as CMOS.

The radiation damage to a cylindrical vertex detector caused by charged particles from the primary reaction can be estimated¹ by assuming that $dN/d\eta$ is constant over the length of the vertex detector. Assume that a “RHIC year” is 10^7sec long at a Luminosity²⁹ of $2 \times 10^{20}\text{cm}^{-2}\text{sec}^{-1}$ with $\sigma_{tot} = 6.13\text{b}$. For central Au+Au collisions assume that $dN/d\eta$ for charged particles is constant at ≈ 800 in the central region (see fig. 3). For minimum-bias Au+Au events this would be reduced to ≈ 200 . With these assumptions, the radiation damage per “RHIC year” can be estimated:

$$\frac{\text{Dose}}{\text{time}} \approx \frac{125\text{Gy/year}}{R_1^2} \quad (4)$$

where R_1 is the radius of the cylinder in cm and $1\text{Gy} = 100\text{Rad}$. This is a factor of ≈ 3000 less than at the SSC and should not cause a serious problem if radiation hard electronics are used. For example, tests with the CDF SVX-1 detector¹¹, without radiation hard electronics, showed a doubling of the electronic noise for a dose of 20Krad . At RHIC, a dose of $\approx 350\text{Rad}$ per “RHIC year” would be expected — far below this limit. Therefore, radiation damage

should not be a problem at RHIC. Neutral particles and the presence of a magnetic field around the vertex could increase this dose, but the estimate suggests that it will not be important.

9 Conclusions

The simulations show that a vertex detector like the one described here will be able to measure the charged particle multiplicity except for very low multiplicity events, where statistical effects in the sampling of the distribution limit the measurement. The detector will be able to measure $dN/d\eta$ in all cases studied as long as the noise is understood. The noise will be an important factor in the multiplicity and $dN/d\eta$ measurements for p+p and p+Au.

On-line vertex finding with high efficiency is possible using the correlation method for central Au+Au events. Offline, the pseudo-tracking method should have $\approx 100\%$ efficiency in this case. The correlation method can not determine the vertex on-line for p+Au or p+p because the multiplicities are too low but the pseudo-tracking method finds the vertex in 90% or more of the p+Au events and 70% or more of the p+p events. The pseudo-tracking method breaks down for charged particle multiplicity less than ≈ 10 , and is affected by the noise in the detector.

A vertex detector with reduced coverage⁷ would make the already marginal measurement of the multiplicity in p+p and p+Au worse, but a trigger-level multiplicity may not be needed for these collisions. For an easily interpretable multiplicity measurement, at least one segment of strips parallel to the beam should remain in the system, as the angle of incidence of the particle makes it difficult to extract meaningful multiplicities (or $dN/d\eta$) from the perpendicular strips. The last 14% in vertex finding efficiency that comes with the more complete vertex detector for p+p and 8% for p+Au (compare tables 3 and 4) may not be worth the extra cost of an extra azimuthal segment. However, it is the η coverage out to $\approx \pm 3$ and the correlation method for finding the vertex which constrain the length of the detector. Reducing the length of the detector will make the correlation method fail more often, eliminating the possibility of a high-resolution high-efficiency on-line vertex reconstruction. For comparison, a 100cm long detector covers 97.7% and a 132cm detector covers 85.4% of the Au+Au interaction diamond. If the inefficiency at the ends is acceptable, a shorter length for the azimuthal segments with perpendicular strips could be used. For 100cm long azimuthal segments with parallel strips, the η coverage is maintained.

Another potentially valuable feature of the parallel strips is finding the vertex position in the transverse direction. The transverse size of the beam should be very small ($\sigma \approx 0.45\text{mm}^{1/2}$) for Au+Au), but the ability to measure the beam

position in the transverse direction could be extremely useful in the alignment of the detector.

There are still some problems with the vertex detector that require further study. Thermal expansion and contraction of the detector (and its support structure) are important and related to the power dissipation by the electronics. These effects are being studied and will constrain the electronics design. A study of electronics components with low power dissipation is underway. Some sample detectors and electronic components have been acquired and are in the process of being tested as a system.

10 REFERENCES AND NOTES

1. For a brief summary of the characteristics of Si strip detectors see: Particle Data Booklet, 1990 edition, pg 131; M. Aguilar-Benitez, *et. al.*, Phys. Lett. **B239**, i (1990).
2. S. Aronson et.al., "A Lepton/Photon Spectrometer for RHIC, Measurements of Lepton Pairs, Vector Mesons, and Photons," letter of intent: July 15, 1991.
3. B. Nilsson-Almqvist and W. Stenlund, Comput. Phys. Commun. **43**, 387 (1987); the calculation here used: Standard Lund parameters, \sqrt{s} 200.0GeV. Fritiof version 1.7, Jetsset version 6.3.
4. ROHACELL is a registered trademark. Available from Rohm Tech Inc. 195 Canal St. Malden, MA 02148. It is a polymethacrylimide foam.
5. D. Beavis, *et. al.*, Fourth Workshop on Experiments and Detectors for a Relativistic Heavy Ion Collider, BNL report # 52262, 235 (1990), M. Fatyga and B. Moskowitz, eds.
6. P. L. McGaughey, private communication. The vertex detector used in E789 at Fermilab is based on 50 μ m pitch Si strips. This (currently operating) detector has ~90% efficiency for an individual strip with about 1/1000 strips "on" due to noise.
7. TALES/SPARHC Letter of Intent for a RHIC Experiment, P. H. Zhang et. al. July 1991.
8. A binomial distribution is appropriate if the probability that a particle will hit the vertex detector is the same for each particle and independent of the others.
9. RHIC Bulletin, BNL, Vol. II, No. 3, Oct. 1991

10. D. Christian, *et. al.*, IEEE Trans. on Nucl. Sci., NS-36, 507 (1989).
11. CDF vertex detector: W. C. Carithers, *et. al.* , Nucl. Inst. Meth. **A289**, 388 (1990).
12. Delphi vertex detector: H. Dijkstra, *et. al.* , Nucl. Inst. Meth. **A289**, 400 (1990); Delphi Collaboration, Nucl. Inst. Meth. **A303**, 233 (1991).
13. Fermilab E687 vertex detector: G. Bellini, *et. al.* , Nucl. Inst. Meth. **A305**, 395 (1991).
14. Mark II vertex detector: C. Adolphsen, *et. al.* , SLAC Report No. SLAC-PUB-5543, 1991 (unpublished); (to be published).
15. Brief descriptions of some existing vertex detectors appear in: Nucl. Inst. Meth. **A305**, 621 (1991).
16. Hamamatsu Photonics K.K. Solid State Division, US address: Hamamatsu Corp. 360 Foothill Road, P.O. Box 6910, Bridgewater, NJ, 08807-0910.
17. Micron Semiconductor Inc., Lansing, England.
18. CSEM, Neuchatel, Switzerland.
19. Ikeda, Japan.
20. L. Van der Have, Silicon Dynamics Inc., Ames, Iowa.
21. Oasis Collaboration, RHIC Letter of Intent, R. Debbé *et. al.* , July 1991.
22. B. Wadsworth, MIT, this conference.
23. C. Britton, ORNL, this conference.
24. S. Kleinfelder *et. al.*, Proc. IEEE NSS Symp. 1987; *ibid*, 1989.
25. G. T. Alley, C. L. Britton, E. J. Kennedy, P. Skubic, ORNL; T. Zimmerman and R. J. Yarema. Some details presented at IEEE Nuc. Sci. Symp., Santa Fe, NM (1991).
26. S. Kleinfelder, LBL, Berkeley, CA. private communication. To be manufactured by UTMCO, Colorado Springs, CO.
27. H. Spieler, LBL, Berkeley, CA.
28. D. Dorfan, S.C.L.P.P., Santa Cruz, CA.
29. S. Ozaki, Nucl. Phys. **A525**, 125c (1991).